Analysis of Linearity Deterioration in Multi-Device RF MEMS Circuits

Umer Shah, *Student Member, IEEE,* Mikael Sterner, and Joachim Oberhammer, *Senior Member, IEEE*

***Abstract*—The paper presents for the first time an RF nonlinearity analysis of complex multi-device RF MEMS circuits. The IIP3 of different RF MEMS multi-device tunable-circuit concepts including digital MEMS varactor banks, MEMS switched capacitor banks, distributed MEMS phase shifters and MEMS tunable filters, is investigated. Closed-form analytical formulas for the IIP3 of MEMS multi-device circuit concepts are derived. A nonlinearity analysis, based on measured device parameters, is presented for exemplary circuits of the different concepts using a multi-device nonlinear electromechanical circuit model implemented in Agilent ADS. The results of the nonlinear electromechanical model are also compared to the calculated IIP3 using derived equations for the digital MEMS varactor bank and MEMS switched capacitor bank. The degradation of the overall circuit linearity with increasing number of device stages is also investigated, with the conclusion that the overall circuit IIP3 is reduced by half when doubling the number of stages, if proper design precautions are not taken. Design rules are presented so that the mechanical parameters and thus the IIP3 of the individual device stages can be optimized to achieve a higher overall IIP3 for the whole circuit. In addition, the nonlinearity of a novel MEMS tunable capacitor concept introduced by the authors, based on a MEMS actuator with discrete tuning steps, is discussed and the IIP3 is calculated using derived analytical formulas.**

***Index Terms*—Intermodulation distortion (IMD), RF MEMS, tunable capacitor, two-tone IIP3 measurement, MEMS varactor.**

I. Introduction

RADIO frequency microelectromechanical system (RF MEMS) tunable and switched capacitors have demonstrated over the years impressive performance in terms of low insertion loss, low power consumption and bandwidth [1], achieving high reliability [2] and a large tuning range [3]. Although packaging and response time are still major challenges to be addressed, these tunable capacitors find applications as tuning elements in phase shifters [4], voltage controlled oscillators, tunable filters [5] and impedance matching networks [6]. These circuits are often operated at moderate to high power levels making linearity an important parameter to avoid signal distortion.

A theoretical and experimental study of the nonlinear effects in RF MEMS varactors and capacitive switches for a single device have been carried out in [7], including analytical derivations and an electromechanical model for verification. Implementations on nonlinearity of the membrane movement of an electrostatically actuated capacitive MEMS switch was also analyzed in [8], using a dynamic and parametric model. A mathematical analysis of the nonlinear behavior of a single MEMS tunable capacitor based on Volterra series has been shown in [9]. An analytical model for computing the intermodulation distortion in a single RF MEMS capacitor made up of two parallel plates has been proposed in [10]. RF circuits operating at high RF power levels create electrostatic forces on the MEMS-tuning mechanisms, which are mechanically-compliant and thus introduce intermodulation distortion. Although these distortions are small for a single device, especially when compared to semiconductor nonlinearities, they grow significantly for complex, multi-device RF MEMS circuits.

The IIP3 of a single RF MEMS shunt capacitor loading on a transmission line is provided in [7]

$$IIP3 = \frac{2kg^2}{\phi C Z_0} = \frac{4kg^2}{\omega C^2 Z_0^2} \tag{1}$$

where k is the spring constant, g is the gap, C is the capacitance between the electrodes, ϕ is the phase, ω is the angular frequency in radians and Z_0 is the characteristic impedance. This equation applies to both digital and analog capacitors in any tuning state. All these previous RF MEMS theoretical nonlinearity analysis have been performed for single devices only. However, state-of-the-art RF MEMS circuits are composed of an increasing number of MEMS-tunable/switched stages and the overall radio receiver, for instance, has to comply to an overall IIP3 limit set by standardization [11], [12]. WiSpry's first generation mobile phone antenna tuner, for instance, has an 80-element MEMS-switched capacitor bank [13]. The nonlinearity effect for a cascade arrangement of circuits is cumulative [14], [15] and the overall IP3 is limited by the lowest value and the nonlinearity of later stages becomes more pronounced because of being scaled down by the gain of the previous stages. This makes it important to analyze the overall nonlinearity of the entire RF MEMS circuit whose IIP3 can differ significantly when compared to a single-stage device. The trend of increase in nonlinear effects in multi-device systems can also be seen in other engineering disciplines [16].

This paper reports on RF nonlinearity analysis of complex multi-device RF MEMS circuits. The nonlinearity analysis is performed for RF MEMS reconfigurable capacitor concepts, *i.e.* digital MEMS varactor bank [17], MEMS switched capacitor bank and an unconventional multi-step switchable varactor, and is further applied to circuit examples of distributed MEMS phase shifters and MEMS tunable filters. The explicit IIP3 equations derived in this paper, though limited to specific MEMS-tuned subcircuits, express the dependency of the over-

The authors are with the Department of Micro and Nanosystems, School of Electrical Engineering, KTH Royal Institute of Technology, Stockholm SE-100 44, Sweden (e-mail: umers@kth.se; msterner@kth.se; joachim.oberhammer@ee.kth.se).

Manuscript received XXXXX; revised XXXXX

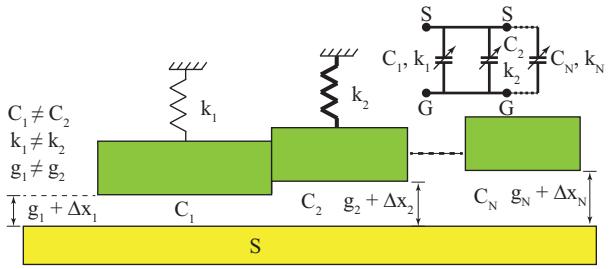

Fig. 1. N-stage capacitor circuit, modeling either N unequal stages or N stages in different operation states.

all circuit linearity on specific design parameters, which is used to understand and formulate design rules for optimizing the overall IIP3 of multi-device RF MEMS circuits. For more complex circuits, a nonlinear electromechanical model in Agilent ADS is used [7], [18] which is compared to the analytical results and to measurement data of circuit examples. Finally, the filter presented in [19] is redesigned based on the proposed design rules to achieve higher IIP3. This paper is a significant extension of a recently published conference paper by the authors [20].

II. Linearity Analysis of Digital MEMS Varactor Bank

Practical RF MEMS circuits, for instance a digital MEMS varactor bank, contain a large number of capacitors. The parameters of the individual MEMS-tunable circuit elements are depending on their operation state, *i.e.* for an overall analysis of the circuit, the IIP3 of all possible states of a circuit should be analyzed, to get the worst-case nonlinearity of the circuit, which is done for the circuit examples in this paper. Fig. 1 shows a circuit model with N parallel capacitor stages which models either a circuit with N different capacitors or a circuit with N equal capacitors in different operating states [21]. Similar to the derivation of a single capacitor in [7], the electrostatic force F_i on the moving electrode of each capacitor C_i, the total capacitance and the phase can be written as

$$F_i = \frac{C_i V^2}{2g_i}, \quad C = \sum_{i=1}^{N} C_i, \quad \phi = \sum_{i=1}^{N} \phi_i \tag{2}$$

N being number of capacitors. The capacitance for a small displacement is

$$C(t) \simeq \sum_{i=1}^{N} C_i \left(1 - \frac{\Delta x_i(t)}{g_i}\right) \tag{3}$$

and the phase is

$$\phi + \Delta\phi = \sum_{i=1}^{N} \phi_i \left(1 - \frac{\Delta x_i(t)}{g_i}\right) \tag{4}$$

When two signals are incident on the capacitor, the output is

$$V_0 = V_1 sin\left(\omega_1 t + \phi + \Delta\phi(t)\right) + V_2 sin\left(\omega_2 t + \phi + \Delta\phi(t)\right) \tag{5}$$

The displacement for each stage can be written as

$$\Delta x_i(t) = \frac{F_i}{k_i} = \frac{C_i}{2k_i g_i}\left[\frac{V_1^2}{2} + \frac{V_2^2}{2} + V_1 V_2 cos(\omega_1 - \omega_2)t\right] \tag{6}$$

The terms $2\omega_1$, $2\omega_2$ and $\omega_1 + \omega_2$ are neglected. Inserting this equation in the above output equation and assuming $V = V_1 = V_2$, the third order intermodulation products can be written as

$$P_{\text{intermod}} = \frac{P_{\text{sideband}}}{P_{\text{signal}}} = \left[\frac{V_1 V_2}{2}\sum_{i=1}^{N}\left(\frac{\phi_i C_i}{2k_i g_i^2}\right)\right]^2 \tag{7}$$

The two-tone third order intermodulation intercept point is the value of P_{signal} for which $P_{\text{signal}} = P_{\text{sideband}}$

$$IIP3 = \frac{2}{Z_0}\left(\frac{1}{\sum_{i=1}^{N}\frac{\phi_i C_i}{k_i g_i^2}}\right) = \frac{4}{\omega Z_0^2}\left(\frac{1}{\sum_{i=1}^{N}\frac{C_i^2}{k_i g_i^2}}\right) \tag{8}$$

Thus, adding an identical second capacitor in parallel to a single-capacitor circuit reduces the overall IIP3 by a factor of two. From (8) it can be generalized that having N number of identical parallel capacitors reduces the IIP3 of the circuit compared to the single capacitor by a factor of N. This is shown in Fig. 2 which analyzes the overall circuit linearity deterioration with increasing number of tunable-capacitor devices, for all circuit states. For this analysis, for each capacitor, the gap is changed from $1.5\,\mu$m to $0.5\,\mu$m, spring constant from 12 N/m to 55 N/m and the capacitance from 45 fF to 145 fF in the up and down states, respectively calculated at the center frequency of 2.5 GHz. A similar analysis can also be performed for series capacitors. Here, the IIP3 also becomes worse as more capacitors are actuated as shown in Fig. 2. This is due to the fact that the IIP3 is directly proportional to the square of the gap which is reduced in the actuated state and inversely proportional to the square of the capacitance which is increased when actuated. This has to be compensated by the spring constant, which is directly proportional to the IIP3, in the down state so as not to reduce the IIP3 substantially in the down state. With adding stages the linearity will remain unchanged if the total capacitance is the same and the spring constant and the gaps are equal for all stages.

It is also noted that if instead of using a digital MEMS varactor bank, a single capacitance is tuned in steps as to achieve the same capacitance of various states of a five stage device shown in Fig. 2, the IIP3 is similar for each state only if the cumulative spring constant and the gap are the same for each state. Designing such a device, as compared to designing a digital MEMS varactor bank, would be difficult since precise control over the spring constant and gap are required in each state.

A 3-bit digital MEMS varactor bank is shown in Fig. 3. The varactors have two discrete positions each with a capacitance ratio of ~ 3. The total capacitance of the circuit can be tuned from 146 fF to 430 fF in eight discrete states. Table I shows the device parameters used for the calculation of the IIP3 for each state. The capacitance values are based on real MEMS device data provided in [17] and the spring constants in the table are derived from the geometries of the membranes by using a COMSOL Multiphysics simulation model. Equation (8) is

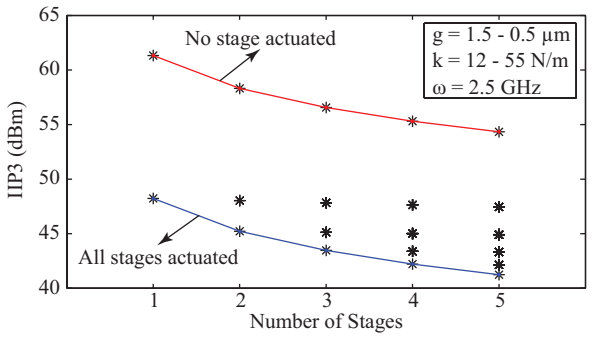

Fig. 2. Change in the overall circuit IIP3 of a digital MEMS varactor bank for all operation states when more capacitor stages are added to the circuit.

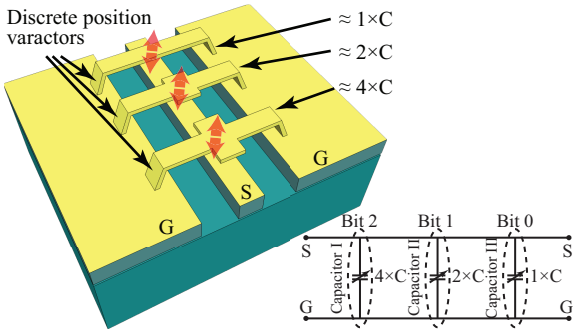

Fig. 3. 3-D illustration and equivalent capacitor model of the three-stage digital MEMS varactor bank.

TABLE I
SUMMARY OF PARAMETERS FOR THREE STAGE DIGITAL MEMS VARACTOR BANK USED FOR LINEARITY ANALYSIS

Parameter	Capacitor I	Capacitor II	Capacitor III
C_{up} (fF)	63	45	38
C_{down} (fF)	205	145	80
g_{up} (μm)	1.5	1.5	1.5
g_{down} (μm)	0.5	0.5	0.5
k_{up} (N/m)	12	12	12
k_{down} (N/m)	55	55	55

used to calculate the IIP3 of the varactor bank in each of its 8 operation states. Fig. 4 shows the calculated IIP3 for the various states of the bank compared to the simulated IIP3 using a nonlinear electromechanical model, similar to [7], implemented in Agilent ADS for each varactor. The simulation data agrees within ±1.7 dBm with the calculated values, confirming the analytical model. The discrepancy between the simulation and calculation is due to the fact that the IIP3 cannot be accurately calculated using the derived equations for large capacitance values. This is because the small capacitance approximation $\omega C Z_0 \ll 1$ used to derive the IIP3 equations is no longer valid for large capacitance values.

III. Linearity Analysis of MEMS Switched Capacitor Bank

MEMS switched capacitor banks are extensively used in tunable filters [22], [23] by using capacitive MEMS switches which are connected in series with high-Q metal-air-metal (MAM) or metal-insulator-metal (MIM) fixed capacitors. By

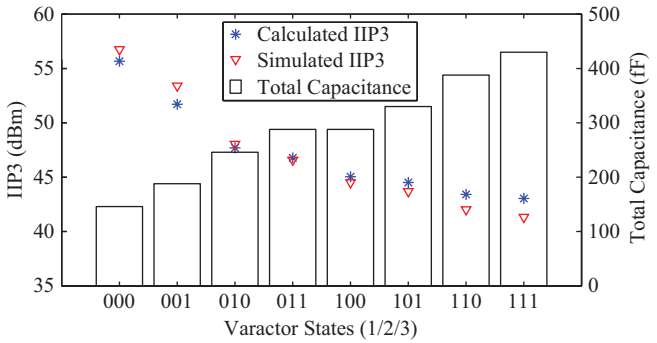

Fig. 4. Calculated and simulated IIP3 of the eight states of the three-stage digital MEMS varactor bank, including the capacitances in the various actuation states.

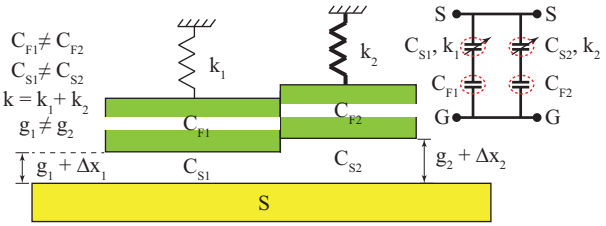

Fig. 5. Two-stage switched capacitor consisting of fixed capacitors (C_{Fi}), which are switched by MEMS capacitive switches (C_{Si}).

choosing appropriate capacitor values of the fixed capacitors, the total capacitor variation can be controlled accurately and a very high capacitance ratio can be achieved.

The MEMS switched capacitor bank can be analyzed using the model in Fig. 5 shown for two stages. The displacement is related to the square of the voltage on the moving MEMS device obtained by using voltage division between the capacitive switch and the fixed capacitor:

$$V_{Si} = \left(\frac{C_{Fi}}{C_{Si}+C_{Fi}}\right) V \tag{9}$$

The displacement can be written as

$$\Delta x_i(t) = \frac{F_i}{k_i} = \frac{C_{Si}}{2k_i g_i}\left(\frac{C_{Fi}}{C_{Si}+C_{Fi}}\right)^2 \left[\frac{V_1^2}{2} + \frac{V_2^2}{2} + V_1 V_2 cos(\omega_1 - \omega_2)t\right] \tag{10}$$

where the terms $2\omega_1$, $2\omega_2$ and $\omega_1+\omega_2$ are neglected. Inserting (10) in (5), the intermodulation level is then given by

$$P_{\text{intermod}} = \frac{P_{\text{sideband}}}{P_{\text{signal}}} = \left[\frac{V_1 V_2}{2}\sum_{i=1}^{N}\left\{\frac{\phi_i C_{Si}}{2k_i g_i^2}\left(\frac{C_{Fi}}{C_{Si}+C_{Fi}}\right)^2\right\}\right]^2 \tag{11}$$

and the calculation of the IIP3 based on the above equation results in

$$IIP3 = \frac{2}{Z_0}\left[\frac{1}{\sum_{i=1}^{N}\frac{\phi_i C_{Si}}{k_i g_i^2}\left(\frac{C_{Fi}}{C_{Si}+C_{Fi}}\right)^2}\right] \tag{12}$$

or

$$IIP3 = \frac{4}{\omega Z_0^2}\left[\frac{1}{\sum_{i=1}^{N}\frac{C_{Si}^2}{k_i g_i^2}\left(\frac{C_{Fi}}{C_{Si}+C_{Fi}}\right)^3}\right] \quad (13)$$

All analytical equations for the overall IIP3 of complex circuits are valid if there is the same voltage across the components in the circuit. If not, the IIP3 of each sub-circuit should be evaluated separately. From the above equations it can be concluded that if the value of the fixed capacitor C_F is large as compared to the capacitive switch C_S then most of the voltage drop is across the capacitive switch, and thus the overall linearity is dominated by the linearity of the MEMS capacitive switch. Similarly for operating states where the fixed capacitor has a small value as compared to the capacitive switch there is less voltage drop across the capacitive switch and thus the influence of the nonlinearity of the MEMS switch on the overall nonlinearity is reduced. The tuning range of the MEMS switched capacitor bank is also limited by the relation $C_{F,LSB} \gg C_{S,up}$ and $C_{F,MSB} \ll C_{S,down}$, where $C_{F,LSB}$ is the fixed capacitor of the least significant bit and $C_{F,MSB}$ is the fixed capacitor of the most significant bit. Thus, there exists a compromise between high tuning range and high IIP3 for the MEMS switched capacitor banks as high tuning range can be achieved with $C_F \gg C_{S,up}$ but at the same time this will result in high voltage drop across the capacitive switch resulting in lower IIP3 as the overall linearity is dominated by the linearity of the MEMS capacitive switch.

Fig. 6 shows an example using a 3-bit MEMS switched capacitor bank. The values of the fixed capacitors are binary coded, *i.e.* doubled from the smallest to the next higher stage. The device parameters used for the analysis are shown in Table II. The up-state capacitance of the MEMS switch is calculated using a 200×100 µm membrane with a gap of 2 µm while the down state capacitance is calculated with a gap of 0.2 µm. The up-state spring constant is calculated by performing simulations in COMSOL Multiphysics for a membrane thickness of 0.8 µm. The down state spring constant is modeled by clamping the membrane at several positions, thus simulating the effect of down-state contact points or spacer bumps, to extract the value of the spring constant. Equation (12) is used to calculate the IIP3 of the switched capacitor bank in each of the 8 operation states. Fig. 7 shows the calculated IIP3 for various states of the bank compared to the simulated IIP3 using the nonlinear electromechanical model of the circuit in Agilent ADS. The simulation of IIP3 agrees within ±2 dBm with the calculated data, confirming the analytical model.

IV. Linearity Analysis of Distributed MEMS Phase Shifter

Distributed MEMS transmission line (DMTL) phase shifters consist of a high impedance line periodically loaded by MEMS bridges. The 2-bit phase shifter example [24] uses MEMS switches in series with fixed MAM capacitors. The first and the second section with seven and fourteen switch stages, respectively, achieve phase shifts of 0^o, 90^o, 180^o and 270^o in the four states. The device parameters used for the IIP3

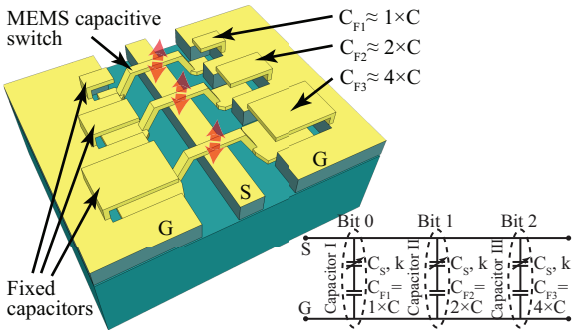

Fig. 6. 3-D illustration and equivalent capacitor model of the three-stage MEMS switched capacitor bank.

TABLE II
Summary of Parameters for Three Stage MEMS Switched Capacitor Bank Used for Linearity Analysis

Parameter	Capacitor I	Capacitor II	Capacitor III
$C_{S,up}$ (fF)	88.5	88.5	88.5
$C_{S,down}$ (fF)	885	885	885
C_F (fF)	160	320	640
$g_{S,up}$ (µm)	2	2	2
$g_{S,down}$ (µm)	0.2	0.2	0.2
$k_{S,up}$ (N/m)	32	32	32
$k_{S,down}$ (N/m)	586.5	586.5	586.5

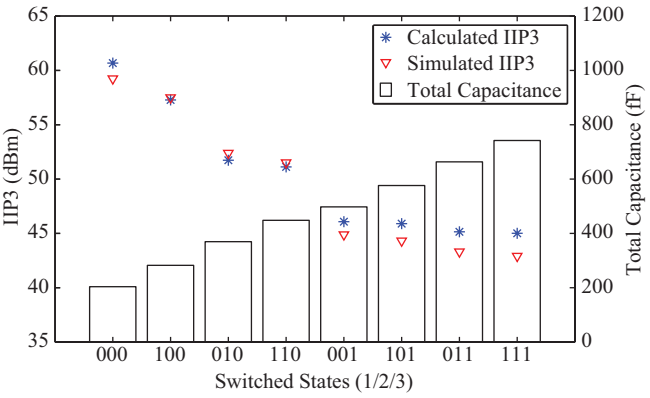

Fig. 7. Calculated and simulated IIP3 of the eight states of the three-stage MEMS switched capacitor bank, including the capacitances in the various actuation states.

analysis are taken from [24]. The down state spring constant is taken from Table II and is modeled by clamping the membrane at several contact points in COMSOL Multiphysics. The IIP3 of the phase shifter is simulated using a harmonic balance simulation of nonlinear electromechanical model for the MEMS switch in Agilent ADS [7]. The results are summarized in Fig. 8 showing the IIP3 of the phase shifter in the four states, the IIP3 of a single switch stage in the up and down state, and the IIP3 of 21 parallel switch stages all either in up or all in down state. It can be deduced from the results that the IIP3 of complex RF MEMS circuits, in this case a DMTL phase shifter, is very different when compared to a single switch stage and even very different when compared to the same number of switch stages in simple parallel combination. Here, the IIP3 of the DMTL phase shifter is much lower than

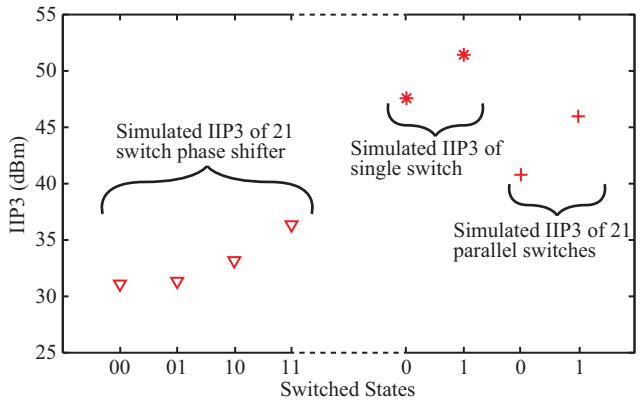

Fig. 8. Simulated IIP3 for the DMTL phase shifter [24] ($f = 13.6$ GHz, $\Delta f = 60$ kHz).

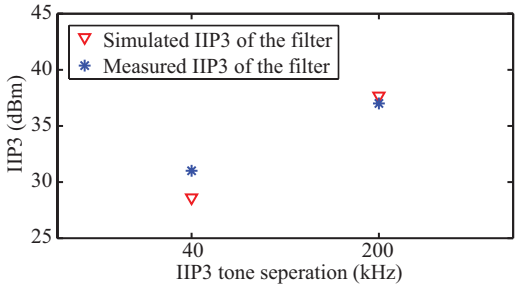

Fig. 9. Simulated and Measured IIP3 for the three-pole filter [19] ($f = 17.8$ GHz, $\Delta f = 40, 200$ kHz).

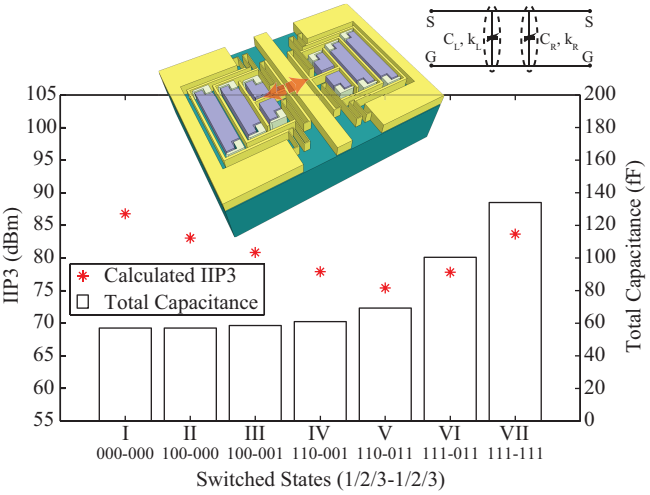

Fig. 10. Calculated IIP3 of the seven states of the multi-step MEMS capacitor ($f = 2.5$ GHz), derived from measured capacitances and the measured geometries of the fabricated device, and the simulated spring constants.

that of a single switch stage and the parallel combination of the same number of switch stages. This emphasizes the need to perform the IIP3 analysis of complex RF MEMS circuits. The nonlinear electromechanical ADS model of a MEMS switch or a MEMS tunable capacitor can be used to simulate the IIP3 of any complex circuit comprising of any components, including through lines, shunt lines, any passives and any number of switches and tunable capacitors with the simulation taking into account the different voltages on the different circuit elements. Such a simulation provides guidance as to what overall IIP3 to expect from any complex RF MEMS circuit in different actuation states.

V. Linearity Analysis of MEMS Tunable Filter

The example of a three-pole filter from [19] can be tuned from 12.2 to 17.8 GHz with each resonator periodically loaded by four switched MEMS capacitor pairs. Every switch is a series combination of a MEMS switch and a fixed MAM capacitor. The loaded MEMS resonators are coupled through inductive inverters to form a three pole band pass filter. The measured IIP3 is compared to simulated IIP3 at the frequency of 17.8 GHz with the tone separation of 40 and 200 kHz using a harmonic balance simulation of nonlinear electromechanical model for the MEMS switch in Agilent ADS [7] with all the switches in the up state. Fig. 9 shows that the simulations agree very well with the measurements. These results confirm the accuracy of the nonlinear electromechanical model implemented in Agilent ADS to precisely predict the IIP3 of the entire RF MEMS circuit. Similar analysis can be performed for any type of multi-device RF MEMS circuits to calculate their IIP3 in all possible actuation states helping to improve the designs in terms of linearity.

VI. Multi-Step MEMS Capacitor

Fig. 10 shows an unconventional MEMS capacitor developed by the authors, based on a 3-D micromachined transmission line with movable ground sidewall sections [21]. The ground-layer embedded laterally stacked actuators split the total movement into multiple, well-defined discrete steps through sequential operation (gap=6.0, 4.67, 3.34, 2 μm, and effective spring constant=211, 94, 73, 5128 N/m, respectively). With asymmetrical actuation, a number of $2n - 1$ states can be achieved with n being the number of single-side actuation stages. The non-linearity of all states of this device has been analyzed using the equations derived in this paper at 2.5 GHz and is shown in Fig. 10, derived from the measured capacitances, measured sidewall displacements and simulated spring constants of the seven states of the device. Equation (1) was used for symmetrical and (8) for asymmetrical actuation, respectively.

VII. Proposed Design Rules

The overall circuit linearity is depending on the number of stages of a MEMS-tuning circuit and proper design precautions have to be taken in order to limit the linearity degradation with increasing circuit complexity, to provide design rules for optimizing the linearity in multi-device RF MEMS circuits. The example of a five stage digital MEMS varactor bank is analyzed. The design variations are implemented so that the total capacitance is unchanged, and the capacitances and springs as described below. For simplicity, only the operation state of all capacitances in the up-state is analyzed.

The capacitance, spring and actuation parameters of different exemplary implementations of a digital MEMS varactor bank are shown in Table III. The initial gap is 1 μm. The IIP3

TABLE III
SUMMARY OF PARAMETERS FOR A FIVE STAGE DIGITAL MEMS VARACTOR BANK USED FOR LINEARITY ANALYSIS

Element	Case I			Case II			Case III			Case IV			Case V		
	C(fF)	k(N/m)	Vp(V)	C(fF)	k(N/m)	Vp(V)	C(fF)	k(N/m)	Vp(V)	C(fF)	k(N/m)	Vp(V)	C(fF)	k(N/m)	Vp(V)
1	198.4	40	7.73	512	40	4.81	512	266.39	12.42	512	103.23	7.73	512	1.04	0.80
2	198.4	40	7.73	256	40	6.80	256	66.60	8.78	256	51.61	7.73	256	4.16	2.19
3	198.4	40	7.73	128	40	9.62	128	16.65	6.21	128	25.81	7.73	128	16.65	6.21
4	198.4	40	7.73	64	40	13.61	64	4.16	4.39	64	12.90	7.73	64	66.60	17.56
5	198.4	40	7.73	32	40	19.25	32	1.04	3.10	32	6.45	7.73	32	266.39	49.66

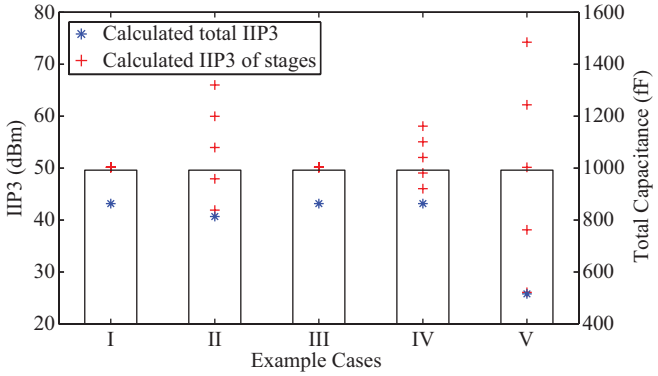

Fig. 11. Calculated IIP3 for the circuits of the five-stage digital MEMS varactor banks, parameters in Table III, given for all actuators in the up state.

of the individual stages of the implementations of the digital MEMS varactor banks are calculated for the up-state using (8) and are shown in Fig. 11, along with the overall capacitance. For Case I, the total capacitance is divided equally among all the stages by having the same value of up state capacitance for each stage. The spring constant is also equal for all the stages which results in an IIP3 of 50.15 dBm and an actuation voltage of 7.73 V for each stage as shown in Fig. 11. The overall IIP3 for this case is 43.16 dBm. For Case II, the capacitor stages are binary coded and the spring constant is the same for each stage and equal to Case I. Here, the IIP3 of all the stages are different and the total IIP3 is 40.67 dBm which is lower as compared to Case I. Here, the actuation voltage for the lowest capacitance is 2.5 times higher than for Case I. For Case III, the capacitances are also binary coded but the spring constants are adjusted such that the IIP3 of each stage is the same and equal to the value of 50.15 dBm, to compare the circuit to the constant-capacitance design of Case I. This is accomplished by using the relationship between k and C of (8) where $IIP3 \propto k/C^2$, and thus adjusting the spring constant accordingly. This strategy results in the total IIP3 for Case III being equal to Case I, despite the binary coding of the capacitances which allows for better tuning resolution. For this case the highest actuation voltage is higher than for Case I but lower than the highest value for Case II showing how to maintain a low actuation voltage while having a high IIP3 for the binary coded case. The actuation voltage variation range is also lower than for Case II. For Case IV, mimicking a design where the spring suspension width is equal to the capacitor-width, the spring constant is divided in the same ratio as the total capacitance is divided among the stages which results in different IIP3 for each stage but the same overall-circuit IIP3 as for Case I and Case III. Here, the actuation voltages are also the same as for Case I. For Case V, the capacitances are again binary coded and the spring constants are taken from Case III but used in the reverse direction. This results in an actuation voltage of 49.66 V in the worst case, *i.e.* a feasible design. The actuation voltage variation range is also the highest for this case. It can be seen here that the total IIP3 is 25.78 dBm which is significantly worse as compared to previous cases, which emphasizes the importance of proper circuit design.

Using these design rules, the three-pole filter in [19] can be redesigned to achieve a higher IIP3. For optimizing the linearity of the filter, the linearity of the MEMS sub circuits *i.e.* the MEMS switched capacitor bank which is utilized for tuning the filter, needs to be optimized. For the implemented design [19], the IIP3 of the MEMS switched capacitor bank is 57.73 dBm and the IIP3 of the filter is 28.58 dBm. For optimizing the IIP3, the switched and fixed capacitance values were not changed and only the spring constant was changed to increase the overall IIP3, in order to preserve the present filter response. The spring constant is increased as to have the maximum actuation voltage of around 46 V and following the design rules above, the IIP3 of each stage is kept uniformly at 67.75 dBm which results in the IIP3 of the bank to be improved from 57.73 to 64.21 dBm. This increases the overall IIP3 of the filter from 28.58 to 34.8 dBm. Adding more flexibility to the design by choosing the capacitance and the switch gap, the overall IIP3 could even be increased further. This example emphasizes the importance of proper IIP3 circuit design.

VIII. CONCLUSION

This paper has investigated the nonlinearity of multi-device RF MEMS circuits. Design recommendations for high linearity of the overall circuit were developed based on analytical formulas derived in this paper. MEMS tunable subcircuits (MEMS varactor banks, MEMS switched capacitor banks, multi-state MEMS capacitor) and circuits based on these elements (phase shifter, tunable filter) have been analyzed. The analytical model, where applicable, agrees well to nonlinear ADS models.

REFERENCES

[1] G. M. Rebeiz, *RF MEMS Theory, Design, and Technology*. NewYork: Wiley, 2003.
[2] A. Grichener and G. M. Rebeiz, "High-reliability RF-MEMS switched capacitors with digital and analog tuning characteristics," *IEEE Trans. Microw. Theory Tech.*, vol. 58, no. 10, pp. 2692–2701, Oct. 2010.

[3] J. Reinke, G. K. Fedder, and T. Mukherjee, "CMOS-MEMS 3-bit digital capacitors with tuning ratios greater than 60:1," *IEEE Trans. Microw. Theory Tech.*, vol. 59, no. 5, pp. 1238–1248, May 2011.
[4] N. Somjit, G. Stemme, and J. Oberhammer, "Binary-coded 4.25-bit W-band monocrystalline-silicon MEMS multi-stage dielectric-block phase shifters," *IEEE Trans. Microw. Theory Tech.*, vol. 57, no. 11, pp. 2834–2840, Nov. 2009.
[5] A. Abbaspour-Tamijani, L. Dussopt, and G. M. Rebeiz, "Miniature and tunable filters using MEMS capacitors," *IEEE Trans. Microw. Theory Tech.*, vol. 51, no. 7, pp. 1878–1885, Jul. 2003.
[6] Q. Shen and N. S. Barker, "Distributed MEMS tunable matching network using minimal-contact RF-MEMS varactors," *IEEE Trans. Microw. Theory Tech.*, vol. 54, no. 6, pp. 2646–2658, Jun. 2006.
[7] L. Dussopt and G. M. Rebeiz, "Intermodulation distortion and power handling in RF MEMS switches, varactors and tunable filters," *IEEE Trans. Microw. Theory Tech.*, vol. 51, no. 4, pp. 1247–1256, Apr. 2003.
[8] D. Mercier, P. Blondy, D. Cros, and P. Guillon, "An electromechanical model for MEMS switches," in *IEEE MTT-S Int. Microwave Symp. Dig.*, 2001, pp. 2123–2126.
[9] M. Innocent, P. Wambacq, H. A. C. Tilrnans, W. Sansen, and H. D. Man, "Measurement of the nonlinear behavior of a MEMS variable capacitor," in *IEEE Int. Conf. Micro Electro Mechanical Systems*, 2004, pp. 773–776.
[10] D. Girbau, N. Otegi, L. Pradell, and A. Lazaro, "Study of intermodulation in RF MEMS variable capacitors," *IEEE Trans. Microw. Theory Tech.*, vol. 54, no. 3, pp. 1120–1130, Mar. 2006.
[11] M. Brandolini, P. Rossi, D. Manstretta, and F. Svelto, "Toward multi-standard mobile terminals - fully integrated receivers requirements and architectures," *IEEE Trans. Microw. Theory Tech.*, vol. 53, no. 3, pp. 1026–1038, Mar. 2005.
[12] C. W. Liu and M. Damgaard, "IP2 and IP3 nonlinearity specification for 3G/WCDMA receivers," *High Frequency Electron.*, vol. 8, no. 6, pp. 16–29, Jun. 2009.
[13] A. S. Morris, Q. Gu, M. Ozkar, and S. P. Natarajan, "High performance tuners for handsets," in *IEEE MTT-S Int. Microwave Symp. Dig.*, 2011, pp. 1–4.
[14] B. Razavi, *RF Microelectronics*. Upper Saddle River, NJ: Prentice Hall, 1998.
[15] T. H. Lee, *The Design of CMOS Radio-Frequency Integrated Circuits*. Cambridge, U.K.: Cambridge Univ. Press, 1998.
[16] J. Pismenny and Y. Levy, "Nonlinear effects of vibration increase in multi-rotor engines," *International Journal of Nonlinear Sciences and Numerical Simulation*, vol. 4, no. 2, pp. 105–124, May 2011.
[17] L. Dussopt and G. M. Reibeiz, "An X- to Ku-band 3-bit digital MEMS varactor," *IEEE Microw. Wireless Compon. Lett.*, vol. 13, no. 9, pp. 361–363, Sep. 2003.
[18] Y. Shim, Z. Wu, and M. Rais-Zadeh, "A high-performance continuously tunable MEMS bandpass filter at 1 GHz," *IEEE Trans. Microw. Theory Tech.*, vol. 60, no. 8, pp. 2439–2447, Aug. 2012.
[19] K. Entesari and G. M. Rebeiz, "A 12-18 GHz three-pole RF MEMS tunable filter," *IEEE Trans. Microw. Theory Tech.*, vol. 53, no. 8, pp. 2566–2571, Aug. 2005.
[20] U. Shah, M. Sterner, and J. Oberhammer, "Analysis of linearity degradation in multi-stage RF MEMS circuits," in *IEEE Int. Conf. Micro Electro Mechanical Systems*, Jan. 2013, pp. 749–752.
[21] ——, "Multi-position RF MEMS tunable capacitors using laterally moving sidewalls of 3-D micromachined transmission lines," *IEEE Trans. Microw. Theory Tech.*, vol. 61, no. 6, pp. 2340–2352, Jun. 2013.
[22] K. Entesari, K. Obeidat, A. R. Brown, and G. M. Rebeiz, "A 25-75 MHz RF MEMS tunable filter," *IEEE Trans. Microw. Theory Tech.*, vol. 55, no. 11, pp. 2399–2405, Nov. 2007.
[23] K. Entesari and G. M. Rebeiz, "A differential 4-bit 6.5-10 GHz RF MEMS tunable filter," *IEEE Trans. Microw. Theory Tech.*, vol. 53, no. 3, pp. 1103–1110, Mar. 2005.
[24] J. S. Hayden and G. M. Rebeiz, "Very low-loss distributed X-band and Ka-band MEMS phase shifters using metal-air-metal capacitors," *IEEE Trans. Microw. Theory Tech.*, vol. 51, no. 1, pp. 309–314, Jan. 2003.

Umer Shah (S'09) was born in Bannu, Pakistan, in 1981. He received the B.Sc. from the GIK Institute, Topi, Pakistan, in 2003, and the M.Sc. degree from the DTU, Copenhagen, Denmark, in 2007. Since 2009, he has been a Ph.D. student with the Department of Micro and Nanosystems, KTH, Stockholm, Sweden. Mr. Shah was the recipient of the Best Student Paper Award presented at the 2010 Asia-Pacific Microwave Conference, Yokohama, Japan.

Mikael Sterner was born in Stockholm, Sweden, in 1981. He received the M.Sc. degree in engineering physics from the KTH Royal Institute of Technology, Stockholm, Sweden, in 2006, and his Ph.D. degree in Microsystem Technology at the KTH in 2012. Currently, he is with COMSOL Inc.

Joachim Oberhammer (M'06-SM'12) was born in Brunico, Italy, in 1976, received his Ph.D. degree from the KTH Royal Institute of Technology, Stockholm, Sweden, in 2004. He became an Associate Professor at KTH in 2007, where he heads a research team with activities in RF/microwave MEMS. He has authored or coauthored over 100 reviewed research papers, six of which having received Best Paper Awards. He holds four patents. Dr. Oberhammer has served as TPRC member of IEEE Transducers, IEEE IMS and IEEE MEMS.